RSC Advances

PAPER

View Article Online
View Journal | View Issue

Cite this: *RSC Adv.*, 2021, **11**, 14154

The dry reforming of methane over fly ash modified with different content levels of MgO†

Yufan Huang,[ab] Qi Li,[ab] Teng Zhao,[ab] Xiaofeng Zhu[ab] and Zijun Wang *[ab]

Received 20th February 2021
Accepted 30th March 2021

DOI: 10.1039/d1ra01381e

rsc.li/rsc-advances

Large amounts of industrial waste fly ash (FA) have caused serious pollution to the environment. There are a few reports that this kind of material, with its good thermal stability, can be used as a catalyst support for high-temperature catalytic reactions, and it has a certain application space. Upon the alkali treatment of fly ash, its specific surface area is increased, and it has the potential to be a catalyst support. Using treated fly ash as the carrier, a nickel-based catalyst was prepared *via* a sol–gel method, and the catalytic performance changes of catalysts with different MgO content levels in the dry reforming of methane are discussed. Under the conditions of a space velocity of 1.8×10^4 mL g^{-1} h^{-1} and a reaction temperature of 750 °C, in the presence of Ni/NaFA-M2 (M2 = 20 wt% MgO), the CH_4 conversion rate can reach 84%, and it has good reaction stability. This will provide a way to use fly ash and carry out more research.

1. Introduction

Excessive coal combustion and industrial production have caused a large amount of greenhouse gas emissions and brought about the greenhouse effect, which has restricted the development of society and seriously endangered the living environment of human beings. At the same time, among greenhouse gases such as CO_2, N_2O, and CH_4, CO_2 accounts for 76% of the world's total greenhouse gases,[1] and it has good stability and has been considered the most polluting gas. In this context, dry methane reforming (DRM) technology has become a research hotspot. This method can make two prevalent kinds of greenhouse gas, CO_2 and CH_4, react to generate clean energy in the form of H_2 and CO. Compared with partial oxidation or steam reforming, the synthesis gas ratio of H_2/CO is close to 1.[2] It can be used in the Fischer–Tropsch synthesis reaction. Under appropriate conditions, it can synthesize liquid fuel mainly based on paraffinic hydrocarbons. To a certain extent, it can solve the problems of the energy crisis and environmental pollution caused by global warming.

The main reaction formula of methane dry reforming is

$$CO_2 + CH_4 \rightarrow 2CO + 2H_2,\ \Delta H_{298\ K} = +247\ \text{kJ mol}^{-1}, \quad (1)$$

but in addition to the main reaction, the following side reactions may also exist:[3]

Methane cracking reaction:

$$CH_4 \Leftrightarrow C + 2H_2,\ \Delta H_{298\ K} = +75\ \text{kJ mol}^{-1}, \quad (2)$$

Reverse water gas reaction:

$$CO_2 + H_2 \Leftrightarrow CO + H_2O,\ \Delta H_{298\ K} = +41\ \text{kJ mol}^{-1}, \quad (3)$$

Carbon monoxide disproportionation reaction:

$$2CO \Leftrightarrow C + CO_2,\ \Delta H_{298\ K} = -171\ \text{kJ mol}^{-1}, \quad (4)$$

The DRM reaction is an endothermic reaction (eqn (1)). In most cases, the reaction requires a temperature above 643 °C to achieve a high equilibrium of CO_2 and CH_4 conversion into H_2 and CO synthesised gas.[4] In this reaction, many studies have confirmed that the use of nickel as an active component to prepare a catalyst can give it good catalytic activity and stability. From an industrial point of view, compared with precious metals, low-cost, high-reserve nickel-based catalysts have more advantages. They have higher economic application prospects. However, under high-temperature reaction conditions, the active component nickel is prone to sintering and produces carbonaceous deposits. The carbon deposits may mainly come from the methane cracking reaction (eqn (2)) or the carbon monoxide disproportionation reaction (eqn (4)). This causes rapid deactivation of the catalyst. Therefore, various methods have been developed to improve the sintering resistance and carbon deposition resistance of the catalyst. Through the catalyst preparation method,[3,5–7] active component loading content,[8] carrier modification method,[9–11] additives[12] and other means affecting the catalyst structure, the active component

[a]*School of Chemistry and Chemical Engineering, Shihezi University, Shihezi, Xinjiang, 832003, PR China. E-mail: eavanh@163.com; lqridge@163.com; 1175828694@qq.com; 318798309@qq.com; wzj_tea@shzu.edu.cn*

[b]*Key Laboratory for Green Processing of Chemical Engineering of Xinjiang Bingtuan, Key Laboratory of Materials-Oriented Chemical Engineering of Xinjiang Uygur Autonomous Region, Engineering Research Center of Materials-Oriented Chemical Engineering of Xinjiang Bingtuan, Shihezi, Xinjiang, 832003, PR China*

† Electronic supplementary information (ESI) available. See DOI: 10.1039/d1ra01381e

particle size, catalyst pH and other aspects can be changed to improve the catalyst performance. The addition of alkali metals or alkaline earth metals such as MgO, CaO, or BaO to the catalyst can adjust the acidity and basicity of the catalyst, reduce the particle size of the active component and enhance the metal-support interaction (MSI), thereby effectively reducing the sintering of active components and inhibiting carbon deposition to a certain extent.[13–15] Sogand Aghamohammadi *et al.*[16] studied the influence of the sol–gel method and the conventional impregnation method on nickel-based catalysts in the dry reforming of methane. The results show that a catalyst NiO prepared by the sol–gel method has better dispersibility, and the catalyst has better catalytic activity and carbon deposition resistance. Therefore, we chose the sol–gel method as the catalyst preparation method.

Fly ash (FA) is an industrial waste discharged from coal-fired power plants. It is a mixture of crystals, glass and a small amount of unburned charcoal with a composite structure. The development and utilization of low-cost fly ash is a good choice for protecting the ecological environment and opening up new economic opportunities. Both SiO_2 and Al_2O_3 are common catalyst supports. The initial activity of a catalyst prepared with SiO_2 as the carrier is relatively low.[17] Although a catalyst prepared with Al_2O_3 as the carrier has higher initial activity, the surface properties of Al_2O_3 are that it is acidic and has weak CO_2 adsorption capacity, so the catalyst is prone to carbon deposition and deactivation.[18] Fly ash is mainly composed of amorphous SiO_2, Al_2O_3 and other oxides.[19,20] The presence of a high content of SiO_2 and Al_2O_3 gives fly ash good thermal stability, and it is used as a catalyst carrier, and is widely used in various reaction fields. Vikranth Volli *et al.*[21] used fly ash as a carrier and added waste animal bone meal to synthesize a transesterification catalyst. Lei Gong *et al.*[22] used fly ash as a carrier to synthesize a solid acid catalyst for the production of furfural from the hydrolysate of corn stover. Pramendra Gaurh *et al.*[23] used fly ash to synthesize a low-cost natural catalyst. Shurong Wang *et al.*[24] used fly-ash-supported nickel as a catalyst. The catalyst has good activity at 700 °C and the stability time can reach more than 10 hours. Therefore, fly ash has the potential to become a catalyst support for the methane dry reforming reaction.

In this study, in order to increase the specific surface area of fly ash and make it a suitable carrier for the DRM reaction, NaOH and HCl solutions were selected to activate and characterize fly ash. To improve the catalytic performance of the Ni based catalyst, alkali metal oxide MgO was added. It is reported that MgO can form a solid solution with NiO because its crystal structure is similar to NiO, so as to improve the sintering resistance of the catalyst. In addition, it has a good reduction temperature, increases the alkalinity of the catalyst, improves the adsorption of acidic CO_2 by the catalyst, and can achieve the purpose of increasing the activity of the catalyst.[25–27] By adding MgO and activated fly ash to the composite, loading the active component nickel, and using the sol–gel method to synthesize Ni/NaFA-MgO catalysts, the catalysts obtained under different MgO contents were extensively characterized and catalytic activity research conducted. This research may provide a new approach for FA treatment and develop a cheap and efficient methane dry reforming catalyst with potential industrial application value.

2. Experimental

2.1 Synthesis of MgO incorporated fly ash composite (FAMgO)

Fly ash (FA) was used in a control experiment, and different solutions were used to modify it. FA was placed in 2mol L^{-1} NaOH solution and 2mol L^{-1} HCl solution at a solid–liquid ratio of 1 : 10, and then the mixture was reacted at 100 °C for 24 hours. Then the FA was cooled to room temperature, filtered, washed until neutral and dried to obtain treated fly ash (NaFA). The final fly ash was then subjected to physical and chemical analysis. The chemical composition of fly ash is shown in Table 1. Appropriate products were selected for the follow-up experiments.

1 g of urea was dissolved in 40 mL of deionized water and 1.5 g of magnesium acetate was dissolved in 50 mL of deionized water, respectively, and then the two solutions were mixed and stirred for 30 minutes. Subsequently, 0.9858 g of NaFA was added to the above mixed solution and stirred at room temperature for 5 hours, and then the mixed solution was stirred at 80 °C until it became a sol–gel. After drying overnight, it was calcined at 200 °C for 2 hours to finally obtain NaFA-30% MgO. According to the above method, NaFA-10% MgO and NaFA-20% MgO were prepared respectively as catalyst supports.

2.2 Catalyst preparation

Ni/NaFA-MgO catalysts modified with different proportions of MgO were prepared by the sol–gel method. The catalysts containing 10%, 20% and 30% MgO are referred to as Ni/NaFA-M1, Ni/NaFA-M2 and Ni/NaFA-M3, respectively. First, an appropriate amount of $Ni(NO_3)_2 \cdot 6H_2O$ and citric acid was dissolved in a small amount of deionized water to prepare an Ni precursor. A certain amount of NaFA was added to 30 mL of deionized water, stirred at room temperature for 15 minutes, and then the mixture was added to the precursor solution, stirred at 80 °C, and a small amount of polyethylene glycol 400 added after 30 minutes. It was further stirred until it became a sol–gel, heated in an oven for 24 hours, and then calcinated at 750 °C for 4 hours to prepare the catalyst. The nickel loading was 12%. The preparation process is shown in Fig. 1.

2.3 Catalytic reaction tests

The performance test of the catalyst was carried out on a micro fixed-bed reactor. The test process was as follows: a certain

Table 1 Chemical compositions of fly ash samples

	Mass (%)		
Constituent	FA	FA-NaOH	FA-HCl
SiO_2	52.75	44.50	59.62
$Al2O_3$	31.98	31.02	32.09
Na_2O	0.56	12.48	0.42
Fe_2O_3	4.60	4.09	2.31
CaO	4.40	4.40	1.21
K_2O	2.07	0.55	2.04
TiO_2	1.24	1.00	1.18
Specific surface area (m^2 g^{-1})	2.4	59.5	18.5

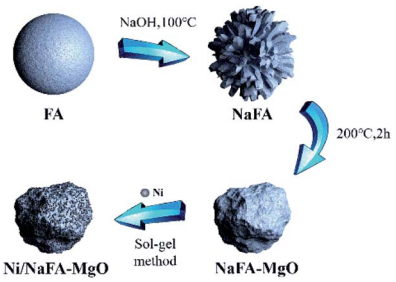

Fig. 1 A catalyst-preparation flow chart.

amount of catalyst was weighed with a size of 40–60 mesh and mixed with 6 times the mass of quartz sand of the same mesh. Before the reaction, it was purged with N_2 for 10 minutes, and then a 5 vol% H_2–Ar mixed gas with a flow rate of 50 mL min^{-1} was used to reduce it at 800 °C for 2 hours. After the reduction, the temperature was changed to the required reaction temperature of 750 °C, and a mass flow meter was used to control the flow rates of CO_2 and CH_4 ($CH_4 : CO_2 : N_2 = 1 : 1 : 1$). The reactant conversion rate and product distribution were tested at a space velocity of 1.8×10^4 mL g^{-1} h^{-1} and 750 °C. A GC-9790 gas chromatograph was used for online analysis, and a TDX-01 packed column was used to separate H_2, N_2, CO, CO_2 and CH_4. The carrier gas was high-purity Ar, the flow rate was 30 mL min^{-1}, and TCD detection was used.

3. Results and discussion

3.1 Physical and chemical characteristics of treated fly ash

The chemical composition of the sample is shown in Table 1. The main components of fly ash are oxides of Si and Al, as well as various other oxides. It can be seen from Fig. 2 that after HCl treatment, the surface of the FA microspheres did not change significantly, while the specific surface area of FA increased. As shown in Table 1, after treating fly ash with HCl, the Fe_2O_3 content in FA decreased from 4.99% to 2.31%, while the CaO content decreased from 4.78% to 1.21%, resulting in a relative increase in SiO_2 and Al_2O_3 content. The main reason for the decrease in Fe_2O_3 and CaO content is that the neutralization between Fe_2O_3, CaO and HCl leads to the dissolution of Fe_2O_3 and CaO. After alkali treatment, the main components of untreated fly ash FA and HCl-treated fly ash are similar, while the Na content in fly ash treated with NaOH is significantly increased. Since NaOH reacts with FA, SiO_2 and Al_2O_3 to form silicate, it still contains a large amount of Na after washing NaFA to neutrality. In Fig. 2, it is found that NaOH solution affects the properties of FA by deforming the spherical shape and transforming its smooth surface into crystals of various shapes (such as flakes and rods). The flakes and rods on the FA surface are generated zeolite substances. This is confirmed in the XRD data of this experiment. As shown in Fig. 3, the appearance of $Na_{3.552}(Al_{3.6}Si_{12.4}O_{32})(H_2O)_{10.656}$ P-type zeolite and $Na_6Al_6Si_{10}O_{32}$ sodium aluminosilicate is observed. The results are similar to those reported by P. Pengthamkeerati *et al.*,[28] which indicates that fly ash can be transformed into zeolite materials and silicate materials

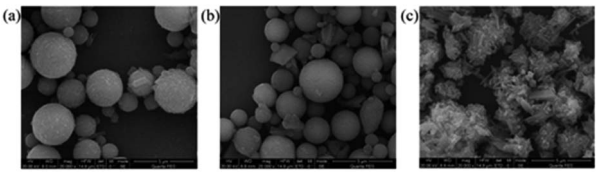

Fig. 2 SEM images of fly ash: (a) untreated original fly ash, (b) HCl-treated fly ash, and (c) NaOH-treated fly ash.

under alkaline conditions. At the same time, the specific surface area of FA after alkali treatment has been significantly increased. This is the result of the conversion of fly ash into a zeolite-like structure under alkaline conditions.[28]

3.2 XRD

Fig. 3 shows the XRD patterns of fresh catalysts synthesized with different MgO composite amounts at $2\theta = 10–90°$. The catalysts containing 10%, 20% and 30% MgO are referred to as Ni/NaFA-M1, Ni/NaFA-M2 and Ni/NaFA-M3, respectively. In Fig. 3, we can clearly see the crystallization peak of NiO, indicating that NiO has been successfully loaded on NaFA. As we all know, as the content of MgO increases, Mg^{2+} will diffuse into the NiO lattice and move to a low angle according to Vegard's law. This can indicate that under the interaction of NiO and MgO, the two can form a solid solution to achieve the purpose of controlling Ni particle size.[29,30] It can be seen from Table S1† that the particle size of Ni is smaller than that of Ni/NaFA after reduction at 800 °C after adding MgO. Furthermore, NiO(200) in Ni/NaFA-M1 appears at 43.0°, which is lower than the diffraction angle of pure NiO(200). This indicates that Mg^{2+} diffuses into the NiO lattice, so there may be "free" NiO or NiO-based NiO–MgO solid solution in Ni/NaFA-M1. At the same time, the position of the NiO(200) diffraction peak in Ni/NaFA-M2 and Ni/NaFA-M3 is also lower than that of NiO(200) at 43.2°, which proves that Ni^{2+} diffuses into the MgO lattice to form an MgO-based NiO–MgO solid solution.

3.3 FTIR

Fig. S1† shows the FTIR spectrum of the Ni/FA catalyst in the range of 400–4000 cm^{-1}. In this range, at 3300–3600 cm^{-1} were

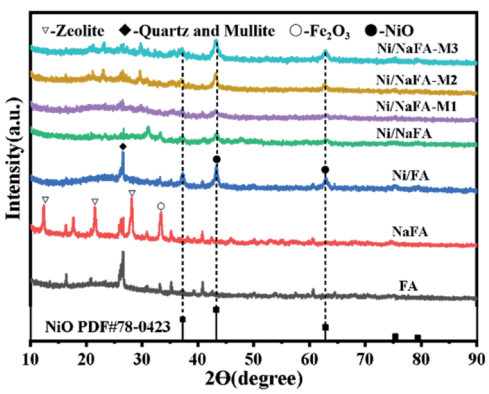

Fig. 3 XRD patterns of fresh catalysts.

observed the surface hydroxyl of Si–OH and the peaks produced by the H–O–H stretching vibration of the surface adsorbed water molecules.[31] The absorption peak in the region of 1500–1750 cm^{-1} is related to the incompletely combusted carbon particles in the fly ash.[32] The peak of the catalyst loaded with Ni disappears here, which may be because the catalyst is calcined at 750 °C. The grain disappeared. A strong absorption peak at 1002 cm^{-1} is caused by the strong asymmetric stretching vibration of Si–O–Si and Al–O–Si tetrahedrons due to SiO_2 as the matrix, which indicates that Al has penetrated into Si–O–Si. A zeolite structure formed in the grid structure. At the same time, compared with untreated FA, the absorption peak of NaFA after alkali treatment shifted to a lower wavenumber direction. This may be due to the substitution of Na^+ for the Si–O–Si and Al–O–Al in the depolymerized silica and alumina tetrahedrons. Some of the groups on the Al–O–Al chain affect their stretching vibration peaks, resulting in a peak shift phenomenon.[32] The shift of the absorption peak of Ni/NaFA-MgO to a smaller wavenumber may be caused by the addition of Mg^{2+}, which depolymerizes the silicate framework structure.[31] The absorption peak observed at 468 cm^{-1} of the catalyst can be attributed to Ni–O and Mg–O. The absorption peaks of FA and NaFA at 441 cm^{-1} belong to the in-plane bending vibration of the Si–O bond. In NaFA, the peak shift may also be caused by the influence of Na^+. In addition, the peak value in the 500–1000 cm^{-1} region may be related to alumina and mineral compounds.[26]

3.4 H_2-TPR

The H_2-TPR characterization results of the catalyst are shown in Fig. 4. Ni/FA and Ni/NaFA have a high and broad peak at 500–850 °C, and the T_{max} for this peak is at around 747.9 °C, which is due to the conversion of Ni^{2+} to Ni element.[33] After adding MgO, the catalyst has a broad single reduction peak between 600 °C and 850 °C, and the T_{max} are about 722.4 °C, 713.4 °C and 719.4 °C, respectively. Due to the interaction between NiO and MgO, the reduction temperature of the Ni/MgO catalyst is lower than that of other catalysts. The reduction peak of the catalyst usually moves to the low-temperature region,[17] and the peak area is significantly reduced, and the reduction peak area of the catalyst increases with the addition of MgO. As the amount increases, the area gradually decreases, and the fraction of reducible Ni decreases with the increase in MgO content.[34–36]

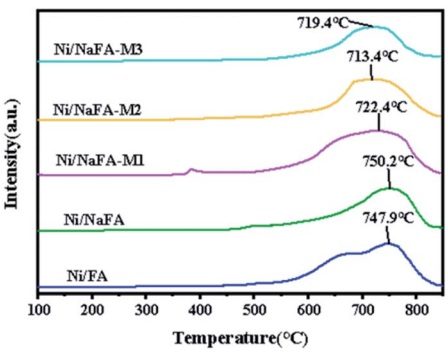

Fig. 4 H_2-TPR curves from the catalysts.

Table 2 Specific surface areas of catalyst samples

Catalyst	S_{BET}[a] (m^2 g^{-1})	Pore volume[b] (cm^3 g^{-1})	Pore width[c] (nm)
Ni/FA	12.3	0.05	16.6
Ni/NaFA	14.4	0.08	19.8
Ni/NaFA-M1	15.8	0.04	9.8
Ni/NaFA-M2	30.1	0.10	10.2
Ni/NaFA-M3	20.9	0.06	9.1

[a] Calculated using the BET equation. [b] BJH desorption pore volume. [c] BJH desorption average pore diameter.

3.5 BET

Table 2 summarizes the specific surface area, pore volume and average pore size of the catalyst. As can be seen, NaOH has an effect on the treatment of fly ash and the MgO content has an effect on the pore size distribution. After the addition of MgO, the specific surface area of the catalyst increased. The specific surface area and pore volume of Ni/NaFA-M2 increased from 12.3 m^2 g^{-1} and 0.05 cm^3 g^{-1} to 30.1 m^2 g^{-1} and 0.10 cm^3 g^{-1}, respectively. This phenomenon is consistent with the report published by J. Ashok.[17] When the MgO content increases to 30%, some MgO species participate in the formation of a non-reducible Ni–Mg-O_x solid solution, resulting in Ni/NaFA-M3, where the specific surface area and pore volume decreased to 20.9 m^2 g^{-1} and 0.06 cm^3 g^{-1}, respectively.[37]

3.6 XPS

The XPS curves of the Ni/NaFA-M1 and Ni/NaFA-M2 spent catalysts are shown in Fig. 5. The chemical oxidation state of Ni metal on the surface of the spent catalysts was measured. Generally for all catalysts, the BE range of Ni $2p_{1/2}$ is 870–878 eV, and the BE range of Ni $2p_{3/2}$ is 850–860 eV.[38] In Fig. 5(a) Ni/NaFA-M1, the spectrum at 855.27 eV represents the oxidation state of Ni, 861.12 eV is the satellite peak of Ni 2p, and the peak near 873.37 eV is the characteristic peak of Ni^{2+} species. The electron transfers from the MgO orbital to the unfilled Ni orbital charges. This electron transfer causes the interaction between MgO and Ni. As shown in Fig. 3, under the interaction of MgO and NiO, the position of the crystallization peak of NiO shifts, inhibiting the agglomeration of Ni and improving the activity of the catalyst.[27] The eV value of the Ni/NaFA-M1 catalyst is lower than that of the Ni/NaFA-M2 catalyst. The higher the BE value, the stronger the interaction between the metal and the support, indicating that Ni/NaFA-M2 has better sintering resistance.[38]

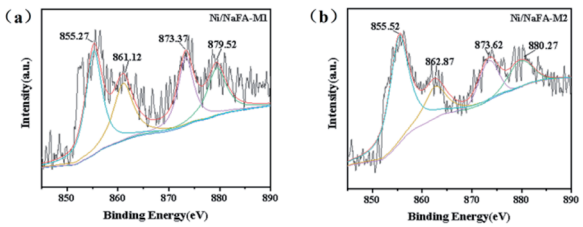

Fig. 5 XPS analysis of spent catalysts: (a) Ni/NaFA-M1 and (b) Ni/NaFA-M2.

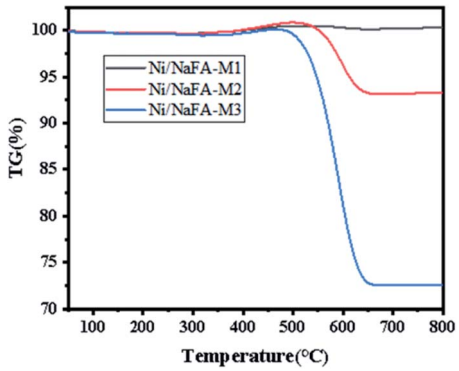

Fig. 6 Thermogravimetry analysis of the catalysts.

3.7 TG

Fig. 6 shows the TG analysis of spent catalysts: Ni/FA-M1, Ni/FA-M2 and Ni/FA-M3. The results show that Ni/FA-M1, Ni/FA-M2 and Ni/FA-M3 have a weight increase at 400–500 °C, which is mainly due to the mass increase caused by the reoxidation of the active metal Ni.[39,40] As the temperature continues to rise, the removal of surface area carbon causes the weight of the sample to drop continuously. Among them, catalyst Ni/FA-M2 shows a weight loss of about 6.7%. Ni/FA-M3 has a relatively large weight loss (about 27.4%), which shows that Ni/FA-M3 has serious carbon deposits. However, Ni/FA-M1 shows no weight loss, indicating that adding 10% MgO to the catalyst gives it better resistance to carbon deposition. The comparison shows that Ni/FA-M1 has the strongest resistance to carbon deposition. With an increase in MgO content, the carbon deposition resistance of the catalyst is gradually weakened.[41] It can be seen from the figure that Ni/FA-M2 and Ni/FA-M3 lose weight between 500 °C and 650 °C. This is due to the oxidation of filamentous carbon, resulting in a weight loss between 500 °C and 650 °C.[42]

3.8 TEM

Fig. 7 shows the TEM images of spent catalysts Ni/NaFA-M1 and Ni/NaFA-M2. It can be clearly seen from the figure that there are carbon nanotubes (CNTs) on the surface of the spent catalyst Ni/NaFA-M2, while there are almost no carbon nanotubes on the surface of Ni/NaFA-M1, which confirms the results from the spent TG catalysts (Fig. 6). At the same time, it is found that adding a small amount of MgO helps to improve the carbon deposition resistance of the catalyst. Even if a large amount of carbon nanotube formation is detected in the sample with 20% MgO content, the stability of the catalyst is still very good, and the conversion rate of CH_4 is maintained at 70% or more.

3.9 Catalytic stability tests

Using methane and carbon dioxide as raw materials, the catalytic dry reforming reaction of methane was carried out at atmospheric pressure and 750 °C. The stability of Ni/NaFA was tested at 750 °C and 1.8×10^4 mL g^{-1} h^{-1}. Fig. 8 shows the effect of MgO on the stability of the Ni/NaFA catalyst. It can be seen that after the FA is modified with NaOH, the specific surface area of the catalyst increases, which has a catalytic effect on CH_4 and CO_2, and the content of MgO in the catalyst increases. The catalyst activity and stability also gradually increase. Among them, the catalyst with 20% MgO has the best catalytic performance and stability, which inhibits the reverse water gas reaction to a certain extent, so that the H_2/CO of the

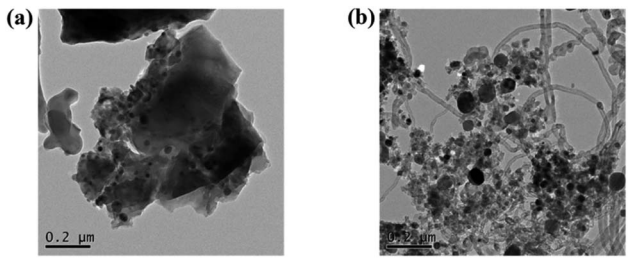

Fig. 7 TEM analysis of spent catalysts after reaction at 750 °C and a CH_4/CO_2 of ratio 1 : 1: (a) Ni/NaFA-M1 and (b) Ni/NaFA-M2.

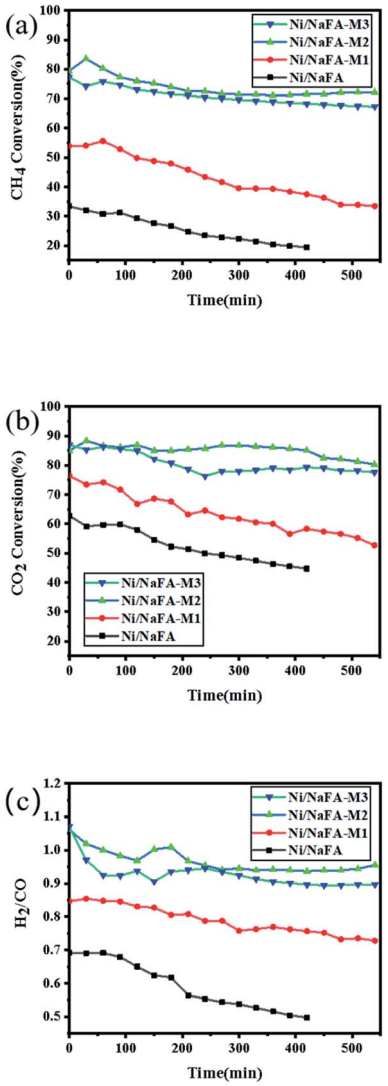

Fig. 8 Catalyst stability at 750 °C for 9 h: (a) CH_4 conversion rate, (b) CO_2 conversion rate, and (c) H_2/CO ratio.

reaction is basically maintained within 540 minutes around 0.95. This is because the basicity of MgO is similar to the crystal structure of NiO. The interaction between the two forms a solid solution, controls the size of Ni, and promotes the adsorption and activation of CO_2, so that the intermediate product reacts with carbon on the catalyst surface to generate CO, thereby increasing the activity and stability of the catalyst.

4. Conclusions

In summary, a series of Ni/NaFA-MgO catalysts was successfully prepared using a sol–gel method. The results show that the use of NaOH to treat fly ash will significantly change the properties of fly ash, and the specific surface area is greatly improved. The sol–gel method was used with the Ni/NaFA catalyst to compound 10%, 20%, and 30% MgO and fly ash. The catalytic performance during the methane carbon dioxide reforming reaction was investigated, and the structure of the catalyst was characterized. The results show that Ni/NaFA-M1 has the lowest carbon deposition, but the catalytic activity is not high. The catalytic activities and stabilities of Ni/NaFA-M2 and Ni/NaFA-M3 are basically the same, and the carbon deposition of Ni/NaFA-M2 is far less than that of Ni/NaFA-M3, and the H_2/CO ratio is closer to 1, showing the best results. XRD results confirmed that there is an interaction between NiO and MgO to form a solid solution, which improves the dispersion of NiO species in the catalyst and achieves the purpose of controlling the Ni particle size. Adding 20% MgO can increase the carbon deposition resistance of the catalyst, give higher catalytic activity, and better inhibit the reverse reaction of water vapor. The carrier has certain industrial application prospects in the methane dry reforming reaction.

Conflicts of interest

There are no conflicts to declare.

Acknowledgements

This work was supported by financial assistance from the National Natural Science Foundation of China [21566031].

References

1 S. Akdag and H. Yıldırım, Toward a sustainable mitigation approach of energy efficiency to greenhouse gas emissions in the European countries, *Heliyon*, 2020, **6**(3), e03396.
2 S. M. Sajjadi, M. Haghighi and F. Rahmani, Sol-gel synthesis and catalytic performance of Ni-Co/Al_2O_3-MgO-ZrO_2 nanocatalyst with different ZrO_2-loadings used in CH_4/CO_2 reforming for hydrogen production, *Int. J. Oil, Gas Coal Technol.*, 2014, **8**(3), 304–324.
3 A. Leba and R. Yildirim, Determining most effective structural form of nickel-cobalt catalysts for dry reforming of methane, *Int. J. Hydrogen Energy*, 2020, **45**(7), 4268–4283.
4 A. S. Al-Fatesh, H. Atia, A. A. Ibrahim, A. H. Fakeeha, S. K. Singh, N. K. Labhsetwar, H. Shaikh and S. O. Qasim, CO_2 reforming of CH_4: Effect of Gd as promoter for Ni supported over MCM-41 as catalyst, *Renewable Energy*, 2019, **140**, 658–667.
5 S. Dekkar, S. Tezkratt, D. Sellam, K. Ikkour, K. Parkhomenko, A. Martinez-Martin and A. C. Roger, Dry Reforming of Methane over Ni-Al_2O_3 and Ni-SiO_2 Catalysts: Role of Preparation Methods, *Catal. Lett.*, 2020, **150**(8), 2180–2199.
6 A. A. S. Oliveira, R. L. B. A. Medeiros, G. P. Figueredo, H. P. Macedo, R. M. Braga, F. V. Maziviero, M. A. F. Melo, D. M. A. Melo and M. M. Vieira, One-step synthesis of $LaNiO_3$ with chitosan for dry reforming of methane, *Int. J. Hydrogen Energy*, 2018, **43**(20), 9696–9704.
7 X. Li, Y. Huang, Q. Zhang, Z. Zuo, X. Wang, V. A. Vinokurov, Z. Wang and W. Huang, Hexamethylenetetramine-assisted hydrothermal synthesis of efficient and stable Ni-MoCeZr-MgAl(O) catalysts for dry reforming of CH_4: effect of Ni content, *Fuel*, 2019, **254**, 9.
8 N. Abdullah, N. Ainirazali, C. C. Chong, H. A. Razak, H. D. Setiabudi, S. Y. Chin and A. A. Jalil, Effect of Ni loading on SBA-15 synthesized from palm oil fuel ash waste for hydrogen production via CH_4 dry reforming, *Int. J. Hydrogen Energy*, 2020, **45**(36), 18411–18425.
9 C. C. Chong, Y. W. Cheng, H. D. Setiabudi, N. Ainirazali, D. V. N. Vo and B. Abdullah, Dry reforming of methane over Ni/dendritic fibrous SBA-15 (Ni/DFSBA-15): optimization, mechanism, and regeneration studies, *Int. J. Hydrogen Energy*, 2020, **45**(15), 8507–8525.
10 A. S. Al-Fatesh, J. K. Abu-Dahrieh, H. Atia, U. Armbruster, A. A. Ibrahim, W. U. Khan, A. E. Abasaeed and A. H. Fakeeha, Effect of pre-treatment and calcination temperature on Al_2O_3-ZrO supported Ni-Co catalysts for dry reforming of methane, *Int. J. Hydrogen Energy*, 2019, **44**(39), 21546–21558.
11 K. Świrk, M. Elena Gálvez, M. Motak, T. Grzybek, M. Rønning and P. Da Costa, Dry reforming of methane over Zr- and Y-modified Ni/Mg/Al double-layered hydroxides, *Catal. Commun.*, 2018, **117**, 26–32.
12 M. Zhang, J. Zhang, Z. Zhou, S. Chen, T. Zhang, F. Song, Q. Zhang, N. Tsubaki, Y. Tan and Y. Han, Effects of the surface adsorbed oxygen species tuned by rare-earth metal doping on dry reforming of methane over Ni/ZrO_2 catalyst, *Appl. Catal., B*, 2020, **264**, 12.
13 X. Y. Gao, K. Hidajat and S. Kawi, Facile synthesis of Ni/SiO_2 catalyst by sequential hydrogen/air treatment: a superior anti-coking catalyst for dry reforming of methane, *J. CO2 Util.*, 2016, **15**, 146–153.
14 Y. Ramezani, F. Meshkani and M. Rezaei, Promotional effect of Mg in trimetallic nickel-manganese-magnesium nanocrystalline catalysts in CO_2 reforming of methane, *Int. J. Hydrogen Energy*, 2018, **43**(49), 22347–22356.
15 S. Liu, L. Guan, J. Li, N. Zhao, W. Wei and Y. Sun, CO_2 reforming of CH_4 over stabilized mesoporous Ni–CaO–ZrO_2 composites, *Fuel*, 2008, **87**(12), 2477–2481.
16 S. Aghamohammadi, M. Haghighi, M. Maleki and N. Rahemi, Sequential impregnation vs. sol-gel synthesized Ni/Al_2O_3-CeO_2 nanocatalyst for dry reforming of methane:

effect of synthesis method and support promotion, *Mol. Catal.*, 2017, **431**, 39–48.

17 J. Ashok, Z. Bian, Z. Wang and S. Kawi, Ni-phyllosilicate structure derived Ni-SiO_2-MgO catalysts for bi-reforming applications: acidity, basicity and thermal stability, *Catal. Sci. Technol.*, 2018, **8**(6), 1730–1742.

18 J. J. Guo, H. Lou, H. Zhao and X. Zheng, Improvement of stability of out-layer $MgAl_2O_4$ spinel for a Ni/$MgAl_2O_4$/Al_2O_3 catalyst in dry reforming of methane, *React. Kinet. Catal. Lett.*, 2005, **84**(1), 93–100.

19 A. R. K. Gollakot, V. Volli and C.-M. Shu, Progressive utilisation prospects of coal fly ash: a review, *Sci. Total Environ.*, 2019, **672**, 951–989.

20 M. Ahmaruzzaman, A review on the utilization of fly ash, *Prog. Energy Combust. Sci.*, 2010, **36**(3), 327–363.

21 V. Volli, M. Kumar Purkait and C.-M. Shu, Preparation and characterization of animal bone powder impregnated fly ash catalyst for transesterification, *Sci. Total Environ.*, 2019, **669**, 314–321.

22 L. Gong, Z. Y. Xu, J.-J. Dong, H. Li, R.-Z. Han, G.-C. Xu and Y. Ni, Composite coal fly ash solid acid catalyst in synergy with chloride for biphasic preparation of furfural from corn stover hydrolysate, *Bioresour. Technol.*, 2019, **293**, 7.

23 P. Gaurh and H. Pramanik, Production of benzene/toluene/ethyl benzene/xylene (BTEX) via multiphase catalytic pyrolysis of hazardous waste polyethylene using low cost fly ash synthesized natural catalyst, *Waste Manage.*, 2018, **77**, 114–130.

24 S. Wang, F. Zhang, Q. Cai, X. Li, L. Zhu, Q. Wang and Z. Luo, Catalytic steam reforming of bio-oil model compounds for hydrogen production over coal ash supported Ni catalyst, *Int. J. Hydrogen Energy*, 2014, **39**(5), 2018–2025.

25 Z. Alipour, M. Rezaei and F. Meshkani, Effect of alkaline earth promoters (MgO, CaO, and BaO) on the activity and coke formation of Ni catalysts supported on nanocrystalline Al_2O_3 in dry reforming of methane, *J. Ind. Eng. Chem.*, 2014, **20**(5), 2858–2863.

26 S. R. Yahyavi, M. Haghighi, S. Shafiei, M. Abdollahifar and F. Rahmani, Ultrasound-assisted synthesis and physicochemical characterization of Ni-Co/Al_2O_3-MgO nanocatalysts enhanced by different amounts of MgO used for CH_4/CO_2 reforming, *Energy Convers. Manage.*, 2015, **97**, 273–281.

27 Y. Xu, H. Long, Q. Wei, X. Zhang, S. Shang, X. Dai and Y. Yin, Study of stability of Ni/MgO/gamma-Al_2O_3 catalyst prepared by plasma for CO_2 reforming of CH_4, *Catal. Today*, 2013, **211**, 114–119.

28 P. Pengthamkeerati, T. Satapanajaru and P. Chularuengoaksorn, Chemical modification of coal fly ash for the removal of phosphate from aqueous solution, *Fuel*, 2008, **87**(12), 2469–2476.

29 Y. H. Wang, H.-M. Liu and B. Q. Xu, Durable Ni/MgO catalysts for CO_2 reforming of methane: activity and metal-support interaction, *J. Mol. Catal. A: Chem.*, 2009, **299**(1–2), 44–52.

30 X. Li, Y. Huang, Q. Zhang, C. Luan, V. A. Vinokurov and W. Huang, Highly stable and anti-coking Ni/MoCeZr/$MgAl_2O_4$-MgO complex support catalysts for CO_2 reforming of CH_4: effect of the calcination temperature, *Energy Convers. Manage.*, 2019, **179**, 166–177.

31 T. H. Vignesh Kumar, V. Sivasankar, N. Fayoud, H. A. Oualid and A. K. Sundramoorthy, Synthesis and characterization of coral-like hierarchical MgO incorporated fly ash composite for the effective adsorption of azo dye from aqueous solution, *Appl. Surf. Sci.*, 2018, **449**, 719–728.

32 Y. Bo, K. Tian-he and K. Jian-ting, Ions-Leaching Rates Rules of Low-Calcium Fly Ash in NaOH Solutions Based on ICP-OES, *Spectrosc. Spectral Anal.*, 2018, **38**(9), 2943–2950.

33 M. Németh, D. Srankó, J. Károlyi, F. Somodi, Z. Schay, G. Sáfrán, I. Sajóc and A. Horváth, Na-promoted Ni/ZrO_2 dry reforming catalyst with high efficiency: details of Na_2O-ZrO_2-Ni interaction controlling activity and coke formation, *Catal. Sci. Technol.*, 2017, **7**(22), 5386–5401.

34 A. S. Al-Fatesh, H. Atia, J. K. Abu-Dahrieh, A. A. Ibrahim, R. Eckelt, U. Armbruster, A. E. Abasaeed and A. H. Fakeeha, Hydrogen production from CH_4 dry reforming over Sc promoted Ni/MCM-41, *Int. J. Hydrogen Energy*, 2019, **44**(37), 20770–20781.

35 B. Huang, X. Li, S. Ji, B. Lang, F. Habimana and C. Li, Effect of MgO promoter on Ni-based SBA-15 catalysts for combined steam and carbon dioxide reforming of methane, *J. Nat. Gas Chem.*, 2008, **17**(3), 225–231.

36 V. R. Bach, A. C. de Camargo, T. L. de Souza, L. Cardozo-Filho and H. J. Alves, Dry reforming of methane over Ni/MgO-Al_2O_3 catalysts: thermodynamic equilibrium analysis and experimental application, *Int. J. Hydrogen Energy*, 2020, **45**(8), 5252–5263.

37 X. Luo, Y. Hong, F. Wang, S. Hao, C. Pang, E. Lester and T. Wu, Development of nano Ni_xMg_yO solid solutions with outstanding anti-carbon deposition capability for the steam reforming of methanol, *Appl. Catal., B*, 2016, **194**, 84–97.

38 K. Bu, S. Kuboon, J. Deng, H. Li, T. Yan, G. Chen, L. Shi and D. Zhang, Methane dry reforming over boron nitride interface-confined and LDHs-derived Ni catalysts, *Appl. Catal., B*, 2019, **252**, 86–97.

39 E. H. Yang, Y. S. Noh, S. Ramesh, S. S. Lim and D. J. Moon, The effect of promoters in $La_{0.9}M_{0.1}Ni_{0.5}Fe_{0.5}O_3$ (M = Sr, Ca) perovskite catalysts on dry reforming of methane, *Fuel Process. Technol.*, 2015, **134**, 404–413.

40 Y.-M. Dai, C.-Y. Lu and C.-J. Chang, Catalytic activity of mesoporous Ni/CNT, Ni/SBA-15 and (Cu, Ca, Mg, Mn, Co)-Ni/SBA-15 catalysts for CO_2 reforming of CH_4, *RSC Adv.*, 2016, **6**(77), 73887–73896.

41 J. Titus, T. Roussière, G. Wasserschaff, S. Schunk, A. Milanov, E. Schwab, G. Wagner, O. Oeckler and R. Gläser, Dry reforming of methane with carbon dioxide over NiO-MgO-ZrO_2, *Catal. Today*, 2016, **270**, 68–75.

42 M. Jafarbegloo, A. Tarlani, A. Wahid Mesbah, J. Muzart and S. Sahebdelfar, NiO-MgO Solid Solution Prepared by Sol-Gel Method as Precursor for Ni/MgO Methane Dry Reforming Catalyst: Effect of Calcination Temperature on Catalytic Performance, *Catal. Lett.*, 2016, **146**(1), 238–248.